 FDMP, vol.1, no.1, pp.1-19, 2005

On the Nature and Structure of Possible Three-dimensional Steady Flows in Closed and Open Parallelepipedic and Cubical Containers under Different Heating Conditions and Driving Forces.

Marcello Lappa[1,2]

Abstract: Possible natural transport mechanisms in cubical and shallow cavities with different heating conditions (from below or from the side) are investigated by means of numerical solution of the non-linear model equations and multiprocessor computations. Attention is focused on a variety of three-dimensional steady effects that can arise in such configurations in the case of low-Pr liquids (silicon melt) even for relatively small values of the temperature gradient due to localized boundary effects and/or true instabilities of the flow. Such aspects are still poorly known or completely ignored owing to the fact that most of the existing experiments focused on the subsequent onset of oscillatory flow, or on the case of transparent ($Pr \gg 1$) liquids. The influence of both buoyancy and surface tension forces is considered. The role played by the geometrical constraints and degrees of freedom in determining the three-dimensional structure of the flow field is discussed. Some effort is devoted to elucidate the results within the framework of existing (state-of-the-art) theories and to illustrate the deviation of results pertaining to a real three-dimensional geometry with respect to earlier two-dimensional models.

keyword: Buoyancy convection, Marangoni flow.

1 Introduction

1.1 Fundamental thermal problems in fluid-mechanics

Natural convection in enclosures and cavities represents a canonical subject of investigation in fluid-mechanics (it has also extensive background application in many branches of materials science). This topic exhibits an outstanding theoretical kinship with the complex of problems that come under the heading of "non-linear dynamics". It, in fact, can be regarded as a good terrain for testing the current ability of fundamental researchers to predict the behavior of complex systems governed by model equations that contain non linear terms in themselves. These flows have been widely studied because of their fundamental interest as possible fascinating models for pattern formation and/or evolution (e.g., Le Quere, 1991); despite the apparent simplicity of the domain where fluid motion arises, an astonishing variety of stages of evolution and final steady or oscillatory regimes is possible; furthermore, discerning of the relevant mechanisms at the basis of flow instabilities in these basic geometrical models is a necessary pre-requisite of any attempt devoted to the precise definition of operating parameters that may provide a stable flow pattern under required technological conditions and/or to the introduction of possible strategies for control of convection.

Obviously, a relevant part of the problem is also represented by the thermal and kinematic conditions along the boundary of the physical domain. They complement the basic partial differential balance equations responsible for the non-linear behavior discussed above, pushing them towards different possible evolutionary progress and the selection of different fundamental mechanisms of convection. Along these lines a first categorization of the possible problems of interest can be introduced as follows: (1) No-slip walls with isothermal horizontal boundaries and adiabatic vertical sides, (2) No-slip walls with adiabatic horizontal boundaries and isothermal (differentially heated) vertical sides, (3) Free adiabatic upper surface and no-slip adiabatic lower boundary with isothermal (differentially heated) vertical sides, (4) Free upper surface with adiabatic vertical sides and isothermal (heated) lower boundary. Case (1) falls into the category of phenomena coming under the heading of Rayleigh-Bènard convection. This type of flow is a basic problem in many industrial heat-transfer systems. An intriguing question is raised by the pattern selection pro-

[1] MARS (Microgravity Advanced Research and Support Center) Via Gianturco 31 - 80146, Napoli, Italy
[2] E-mail: marlappa@marscenter.it, marlappa@unina.it

cess upon which this system evolves through time to a final state.

"The-heated-from-the-side" problem (cases (2) and (3)) has also received much attention over the years. Unlike the heated-from-the-bottom case, the motivation of such an interest is strictly of an application-oriented nature. It is mainly related to the manufacture of bulk semiconductor crystals. The simplest geometry among several crystal growth technologies has, in fact, the horizontal configuration of the Bridgman method, where the convective flow is induced by the horizontal component of the temperature gradient.

Cases (3) and (4) involve the presence of an additional driving force that is basically a gravity-independent phenomenon. If a nonisothermal free surface is involved in the considered problem, then surface-tension forces $\underline{\nabla}_S\sigma$ ($\underline{\nabla}_S$derivative tangential to the interface, σ surface tension) arise that must be balanced by viscous stresses in the liquid. Such a condition enforces a flow by tangential variation of the surface tension (the so-called Marangoni convection). Prior to the space program, this phenomenon had been ignored since on the ground it is often overshadowed by the convective flow of gravitational origin. In microgravity, the reduced level of buoyancy-driven convection allowed Marangoni convection to become obvious. Once it became recognized, however, it was found to be significant in some Earth-based processes as well. Like convection induced by buoyancy forces, it can be an important natural transport mechanism in many hydrodynamic systems (where a free liquid/gas or liquid/liquid interface is involved in the thermal process). In particular, case (4) falls into the category of classical phenomena coming under the heading of Marangoni-Bènard convection.

When the temperature gradient acting on the system (ΔT) reaches a certain critical value, these basic types of convection can undergo transition to a variety of different complex scenarios.

The most fundamental stability analyses of convection flows carried out in the past considered fluid layers of infinite horizontal extent; see, e.g., Busse (1978), Hart (1983), Smith and Davis (1983) and Chandrasekhar (1981) for boundary and heating conditions corresponding to cases (1), (2), (3) and (4), respectively. Because of the light shed on the problem by the subsequent studies (see, e.g., the list of references in Lappa, 2005), however, most of the scientific community is currently aware of

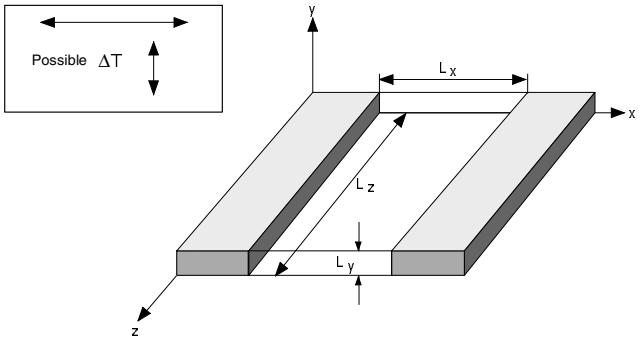

Figure 1 : Sketch of the cavity and of the possible heating directions

the importance that the effective finite geometry of the container may have on the threshold values and observed flow patterns. In many cases, geometrical constraints and the related possible multiplicity of the solutions are essential ingredients of these flows (Gelfgat, 1999). The disturbance wave number is selected out of the full spectrum of disturbances because the single- or multicellular convective structure is closed in a special zone geometry. In many cases, the selection rule is given by the constraint that the wavelength must somewhat be an aliquot of the finite extension of the system.

1.2 Current status, possible improvements and extensions

Many of the existing numerical/experimental studies were carried out for very elongated geometries designed to somewhat mimic the conditions corresponding to the landmark stability analyses cited before (pertaining to the aforementioned unbounded infinite layers). Only a few of them considered systems of very limited extent and many of these were based on two-dimensional (2D) models; this also means that there is still an outstanding lack of information for the case of three-dimensional (3D) domains. Factors like the high computational resources required by the classical algorithms used for these types of problem, the lack of not expensive powerful processors and, more recently, the difficulties arising from the implementation of multi-processor routines (parallel computation) have all combined to limit investigations into the fundamental three-dimensional structure of these flows.

It is thus on these unresolved issues that the present analysis is mainly focused upon. A 3D cubical con-

Table 1 : Physical properties of silicon melt

Melting point temperature T_m [K]	1685
Density ρ [gr/cm^3]	2.42
Thermal diffusivity α [cm^2/s]	2.44×10^{-1}
Kinematic viscosity ν [cm^2/s]	2.45×10^{-3}
Prandtl number	0.01
Thermal conductivity λ [W/cmK]	0.64
Surface tension σ[dyne/cm]	7.33×10^{2}
σ_T[dyne/cmK]	1×10^{-1}

tainer/cavity is selected as the relevant reference case owing to the presence of relatively close boundaries along all the possible directions (x,y and z). In particular, emphasis is given to the role played by the presence of solid constraints along the third direction z (assumed to be infinite in two-dimensional studies). Shallow enclosures ($3\times1\times3$ and $4\times1\times4$) are also investigated (Fig. 1) since their two-dimensional counterparts have been the subject of tremendous interest over past years (mainly as possible benchmarks configurations). Silicon melt (Pr=0.01) is considered as the model liquid (see Table 1) due to its technological importance and since experimental available results mainly concern the case of organic transparent liquids; these fluids are characterized by very large values of the Prandtl number (Pr$\gg$1) and, as summarized in the recent overview of Lappa (2005), tend to behave, in many circumstances, in a very different way with respect to melts of semiconductor materials and liquid metals (the instabilities affecting the related flow often exhibit a very different intrinsic physical nature).

The present analysis, in particular, focuses on the different fluid-dynamic mechanisms (and related "ranges" of applicability) responsible for steady three-dimensional flow and related bifurcations. The few available experimental/numerical three-dimensional studies, in fact, were somewhat limited to the onset of oscillatory convection owing to its relevance to well-known technological processes (e.g., the growth of bulk crystals from the melt) and/or owing to its intrinsic fascinating nature within the context of fundamental studies dealing with problems that come under the heading "route to chaos". For these reasons this article is devoted to a critical and concise analysis of the steady 3D effects. Some effort is provided to illustrate their genesis, the governing nondimensional parameters, the scaling properties, their structure and, in particular, the possible bifurcations to different patterns of symmetry in space (microgravity environment) as well as on the ground. Theoretical arguments introduced over the years by investigators to explain the observed phenomena are used, enriched and fed with new material. Some effort is also provided to clarify still unresolved controversies pertaining to the physical nature of the dominating driving force responsible for possible asymmetric convection in the various thermal systems under investigation. Furthermore, the 3D results are compared with those arising from 2D computations to assess the role played by geometrical constraints in determining edge effects, the overall process of selection of the disturbances and the related symmetries.

2 Physical and mathematical model

2.1 Governing equations and boundary conditions

In the presence of steady gravity (on the ground conditions g=g$_o$ or steady acceleration levels on microgravity platforms) the velocity and temperature can be determined by the differential balance equations (for mass, momentum, and energy).

Following the usual Boussinesq approximation for incompressible fluids, the physical properties are assumed constant, except for the density ρ in the generation term in the momentum balance equation, which is assumed to be a linear function of temperature:

$$\rho = \rho_0 \left[1 - \beta_T \left(T - T_0\right)\right] \tag{1}$$

where β_T is the thermal expansion coefficients, and T$_o$ a reference value for the temperature. In other words, the continuity equation is reduced to the vanishing of the divergence of the velocity field, and variations of the density are ignored in the momentum equation, except insofar as they give rise to a gravitational force.

In the case of thermal problems usually the nondimensional form results from scaling the lengths by a reference distance (L, for the present case it is the height of the computational domain) and the velocity $\underline{V}$ by the energy diffusion velocity $V_\alpha = \alpha/L$ (α is the thermal diffusivity); the scales for time and pressure p are, respectively, L^2/α and $\rho_o\alpha^2/L^2$. The temperature, measured with respect to T$_o$, is scaled by ΔT. This approach leads to:

$$\underline{\nabla}\cdot\underline{V} = 0 \tag{2}$$

$$\frac{\partial \underline{V}}{\partial t} = -\underline{\nabla} p - \underline{\nabla}\cdot[\underline{VV}] + \mathrm{Pr}\,\nabla^2\underline{V} + \mathrm{Pr}\,RaT\underline{i}_g \tag{3}$$

$$\frac{\partial T}{\partial t} = -\underline{\nabla} \cdot [\underline{V} T] + \nabla^2 T \tag{4}$$

and the relevant nondimensional numbers are the well-known Prandtl and Rayleigh numbers (Gr is the Grashof number):

$$\mathrm{Pr} = \frac{\nu}{\alpha} \tag{5}$$

$$Gr = \frac{g \beta_T \Delta T L^3}{\nu^2} \tag{6a}$$

$$Ra = Gr\,\mathrm{Pr} = \frac{g \beta_T \Delta T L^3}{\nu \alpha} \tag{6b}$$

ν is the kinematic viscosity.

The surface tension σ for many cases of practical interest exhibits a linear dependence on the temperature:

$$\sigma = \sigma_o - \sigma_T (T - T_o) \tag{7}$$

where σ_o is the surface tension for T=T_o, σ_T=-d$\sigma/dT > 0$ (σ is a decreasing function of temperature). If a non-isothermal free surface is involved in the considered process, then surface-tension forces arise that must be balanced by viscous stresses in the liquid $\underline{S}\cdot\underline{n}$ ($\underline{n}$ unit vector perpendicular to the free interface, $\underline{S}$ stress tensor). This balance in nondimensional form reads:

$$\frac{\partial \underline{V}}{\partial n} = Ma \underline{\nabla_S} T \tag{8}$$

where

$$Ma = \frac{\sigma_T \Delta T L}{\mu \alpha} = Re\,\mathrm{Pr} \tag{9a}$$

$$Re = \frac{\sigma_T \Delta T L}{\rho \nu^2} \tag{9b}$$

Ma is the so-called Marangoni number (Re is the related Reynolds number); μ is the dynamic viscosity. Since the capillary number ($Ca = \sigma_T \Delta T / \sigma_o$ is very small for all the conditions considered in the present work ($Ca \ll 1$, see Table 1) dynamic surface deformation can be neglected and the melt/air interface is assumed to be flat and undeformable.

2.2 The numerical method

According to the well-known SMAC method (see e.g., Lappa 2002, 2004a) the computation of the velocity field at each time step is split into two substeps.

In the first, an approximate non-solenoidal velocity field $\underline{V}^*$ which corresponds to the correct vorticity of the field is computed at time $(n+1)$ neglecting the pressure gradient term in the momentum eq. (3). In the second substep, the pressure field is computed by solving the equation resulting from the divergence of the momentum equation taking into account eq. (2):

$$\nabla^2 p^n = \frac{1}{\Delta t} \underline{\nabla} \cdot \underline{V}^* \tag{10}$$

For further details on the numerical method see, e.g., Lappa (2002). On the physical boundaries the $\partial p/\partial n = 0$ condition is imposed.

Finally, the correct solenoidal velocity field is updated using the computed pressure field to account for continuity:

$$\underline{V}^{n+1} = \underline{V}^* - \Delta t \underline{\nabla} p^n \tag{11}$$

The temperature distribution at time $(n+1)$ is obtained from eq. (4) after the velocity calculation.

Multiprocessor (Parallel) algorithms are used due to the enormous time required for the computations. Within such a context, the problem is split in two problems, one parabolic and the other elliptic. A parallel algorithm, explicit in time, is utilized to solve the parabolic equations (momentum and energy equations). A parallel multisplitting kernel is introduced for the solution of the pseudo-pressure elliptic equation, representing the most time-consuming part of the algorithm. A grid-partition strategy is used in the parallel implementations of both the parabolic equations and the multisplitting elliptic kernel. A Message Passing Interface (MPI) is coded for inter-processor communications. For the sake of brevity the parallel implementation of this method is not described in detail. For further details on parallel strategies see, e.g., Lappa (2004a) and Lappa (1997).

2.3 Validation and grid refinement study

Validation of the present algorithm has been obtained through quantitative comparison with other recent three-dimensional and steady solutions available in the literature (in Tables 2 and 3, u, v and w represent the velocity components along x, y and z, respectively). In particular, the numerical simulations of Saβ et al. (1995) and of Hof et al. (2004) have been considered as a reference case for what concerns the computation of Marangoni flows and

Table 2 : Validation and grid refinement study, Marangoni convection in cubical cavity, Pr=1, Ma=100, u and T at $x = 0.5, z = 0.5, y = 1$

Grid	u	T
21×21×21	11.15	0.6279
31×31×31	11.058	0.6283
41×41×41	11.027	0.6284
Saβ et al. (1995) (32×32×32)	11.12	0.620

Table 3a: Validation, comparison with the results of Hof et al. (2004), buoyancy convection in laterally heated parallelepipedic cavity (height = 1, length = 5, width = 1.3), Pr=0.0188, Ra=705.

Grid	v_{max}
30×14×16	0.5482
40×18×16	0.5532
Hof et al. (2004) (40×18×16)	0.5386

Table 3b: Grid Refinement study, buoyancy convection in laterally heated cubical cavity, Pr=0.01, Ra=10^3.

Grid	v_{max}	w_{max}
21×21×21	2.075	0.483
31×31×31	2.144	0.428
41×41×41	2.166	0.416

of buoyancy-driven convection, respectively. The simulations carried out for a cubical cavity filled with a Pr=1 liquid and subjected to Ma=100, prove that agreement with the results of Saβ et al. (1995) is obtained within 1% (see Table 2). Table 2 also shows the grid refinement study carried out for the same conditions, from which it is clear that mesh independence can be achieved for a 31×31×31 resolution.

The present results in the case of steady pure buoyancy convection are listed in Table 3a. They coincide within a very small difference (3 %) with those given in the very recent analysis of Hof et al. (2004) (parallelepipedic enclosure with $L_x = 5, L_y = 1, L_z = 1.3$ filled with gallium and Ra=705). The grid independence study for the configuration of interest in the present work (i.e. the differentially heated cubical cavity filled with silicon melt) is given in Table 3b.

According to these preliminary convergence studies it seems that, for relatively small values of the Prandtl number and of the governing characteristic numbers, grid-independence can be easily obtained with a mesh 31×31×31. However, for the sake of high accuracy, all the computations discussed hereafter for the cubical enclosure have been obtained for 51×51×51 grids (this resolution is also somewhat necessary when trying to capture the behavior of a cubical enclosure heated from below at values of the Rayleigh number strongly above the first primary threshold, as also discussed in Puigjaner et al., 2004). The number of computational points has been reduced to 51×21×51 for the shallow cavities. The 2D counterpart of the code has been repeatedly validated through comparison with the results of the GAMM workshop. Second order accurate upwind and central difference schemes have been used for the treatment of the convective and diffusive terms, respectively, in both momentum and energy equations. Thermal diffusive conditions and fluid at rest have been assumed as initial conditions for all the computations.

3 Results

3.1 Rayleigh-Bènard convection

3.1.1 Historical background

By means of studies that considered infinite systems, i.e. the stability of the quiescent state of nonconfined fluid layers heated from below, it is known that the onset of convection is caused by two-dimensional perturbations of the diffusive basic state and that it undergoes instability to couples of counter rotating convective rolls with aspect ratio (ratio of the couple-width to the depth of the layer) $A_c \cong 2$. Currently, however, as mentioned in the introduction, it is well known that if systems confined laterally by rigid sidewalls are considered, even in containers of large horizontal dimensions, the lateral walls can have a significant influence on the flow pattern that develops when the Rayleigh number exceeds its critical value. Thus results for the corresponding infinite layer cannot, in general, be used to make predictions about either the detailed structure or the stability of the roll pattern in practical situations. There are several modes of the most dangerous perturbation which replace each other when the aspect ratio A (ratio of the horizontal extension and of the height of the finite two-dimensional enclosure) is varied. Within this context it should also be mentioned that the increase of the aspect

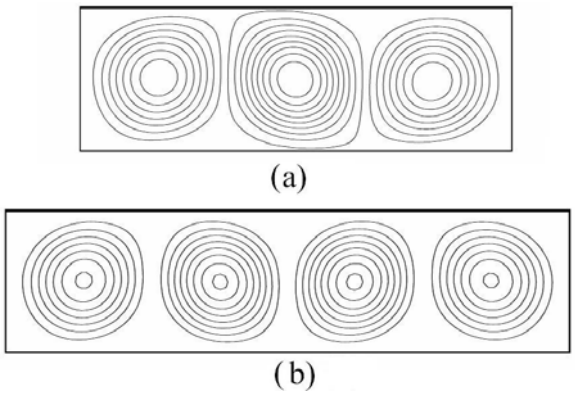

Figure 2 : Two-dimensional rectangular container heated from below and cooled from above with adiabatic sidewalls (Pr=0.01, silicon, Rayleigh-Bènard problem), Ra=3×10^3 (Ra based on the depth of the box): (a) A= 3, (b) A=4.

ratio A generally results in the increase of the number of two-dimensional rolls within the finite-size rectangular container (see the excellent investigation of Gelfgat (1999) for Pr=0 and Pr=0.15). Some results along these lines for the present case of silicon melt (Pr=0.01) are shown in Figs. 2.

3.1.2 Present contribution

When turning to the three-dimensional problem, there are different aspects that would deserve attention. First of all, of course, the analysis of the sensitivity that the final state of the system can exhibit to the presence of limiting sidewalls along the third direction. However, it should be kept in mind that in the specific case of Rayleigh-Bènard convection, as anticipated in the introduction, the possible transitional regimes during the evolutionary progress that leads to the aforementioned final state, also form a relevant and important part of the problem. This aspect, in particular is very poorly known in the case of liquid metals and often the subject of controversies in the literature.

Concerning the first subject of study, interesting insights into the physics of the problem can be obtained by comparing the fields illustrated in Figs.2 with corresponding 3D results. Of course such a comparison makes sense when the domain extension along z is comparable to its extension along x ($L_z/L_x \leq$O(1), whereas in the opposite case of $L_z/L_x >$O(1), 2D results can be regarded as a good approximation of the real flow.

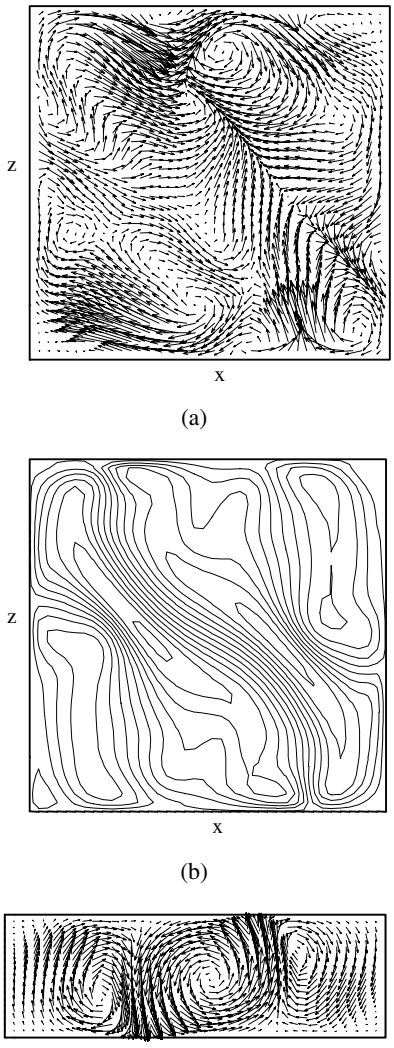

Figure 3 : Rayleigh-Bènard convection in an enclosure with $L_x = 3, L_y = 1, L_z = 3$ (Pr=0.01, Ra=3500, steady state): a) Projection of the velocity field in the horizontal midplane; b) Vertical velocity contours in the horizontal midplane; c) Projection of the velocity field in the xy midplane.

For the enclosure $3 \times 1 \times 3$, a certain apparent degree of 2D behavior can be highlighted for a core zone apparently not affected by edge effects (Fig. 3c). However, Figs. 3a and 3b clearly prove that even if the z-extension is quite large, the flow tends to exhibit a fully three-dimensional structure. After an initial stage, the ensuing steady 3D pattern, in fact, is featured by the presence of parallel convection rolls with a diagonal prevailing direction.

For the 3-D geometry, similarly to the 2-D idealized case, there are several modes of the most dangerous perturbation that replace each other when the aspect ratio is varied. However, the spectrum of possible perturbations is more complicated (Gelfgat, 1999). The larger variety of perturbations is obviously caused by the three-dimensional geometry. Within such a context, the problem becomes even more interesting if a cubical box is considered. In fact, in such a case, an additional complexity is caused by the variety of the symmetries of the system.

Because of the intrinsic symmetry of this configuration the Rayleigh-Bènard flow tends to produce state solutions with manifold symmetries. As the Rayleigh number is increased, new possible patterns of symmetry are prone to occur. Furthermore, as mentioned in the foregoing discussion, the delicate evolutionary route to a final steady state can be coupled to significant and intriguing adjustments in the roll pattern.

According to the analysis of Puigjaner et al. (2004) (carried out in the case of a model fluid with Pr=0.710 (air)), the critical Rayleigh number for the case of a cubical box is Ra_{cr}=3389; such a larger value with respect to the corresponding two-dimensional (square) case $Ra_{cr} \cong 2585$ (Luijkx and Platten, 1981) obviously follows from the presence of solid walls along the third coordinate. It is also worthwhile to stress that these threshold values of the Rayleigh number are affected by the presence of solid constraints but do not depend on the model liquid used for the experiments.

The present results for Pr=0.01 illustrate that among all the combinations, only a stable single x or z roll is possible in the cubical configuration whereas, unlike the cases already discussed for the $3\times1\times3$ container, the diagonal modes $x\pm z$ tend to be unstable, i.e. only appear as transitional stages of evolution. Similar conclusions were also reported by Puigjaner et al. (2004) for Pr=0.710.

Some examples of the possible patterns of symmetry and their ranges of existence in the case of silicon melt are shown in Figs. 4-7. Following Puigjaner et al. (2004) they are categorized as S_i modes with the subscript "i"= 1,2,...,n, and have been obtained as bifurcations from an initial diffusive state. The possible stable flow pattern (S_1 shown in Fig.4), that occurs as a final steady mode of the system in a relatively wide range of the Rayleigh number (Ra_{cr} <Ra< 6×10^4), is formed by one x roll. The S_2 state shown in Fig.5 appears as a transitional solution

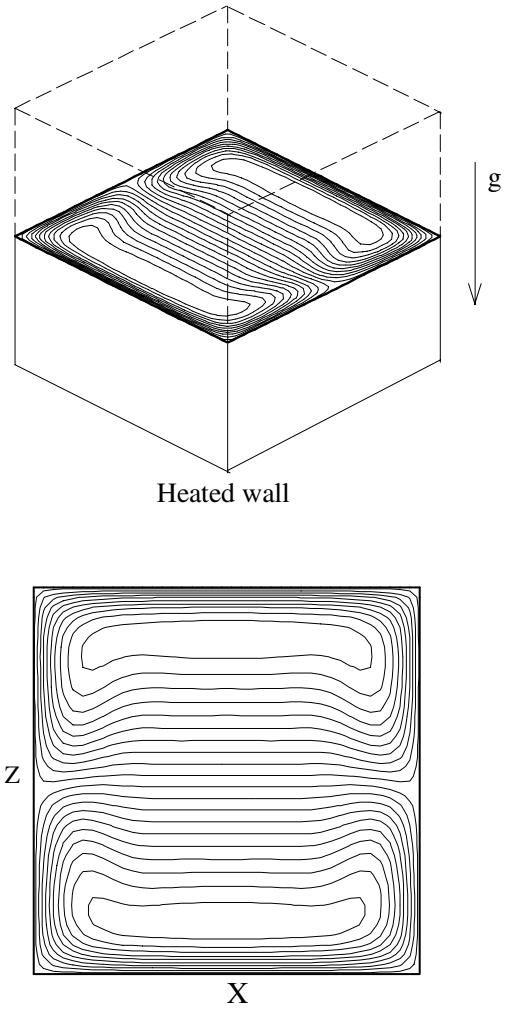

Figure 4 : Vertical velocity contours in the horizontal midplane of a cubical enclosure heated from below with adiabatic vertical walls; pattern of symmetry S_1 (Silicon, Pr=0.01, Ra=5×10^3, steady state).

along the evolutionary process that leads to S_1. It occurs in a limited range of the Rayleigh number (Ra<15000). This S_2 solution can be essentially obtained by subtracting one x roll from one z roll.

For large values of Ra, the transitional S_2 mode is no longer possible and is replaced by a solution with a different symmetry pattern (S_4). The S_4 solution is featured by a toroidal organization of the flow that was also reported by Hernàndez and Frederick (1994) (see Fig. 6).

At very large values of the Rayleigh number (Ra> 7×10^4) a new stable regime can arise. This S_8 structure

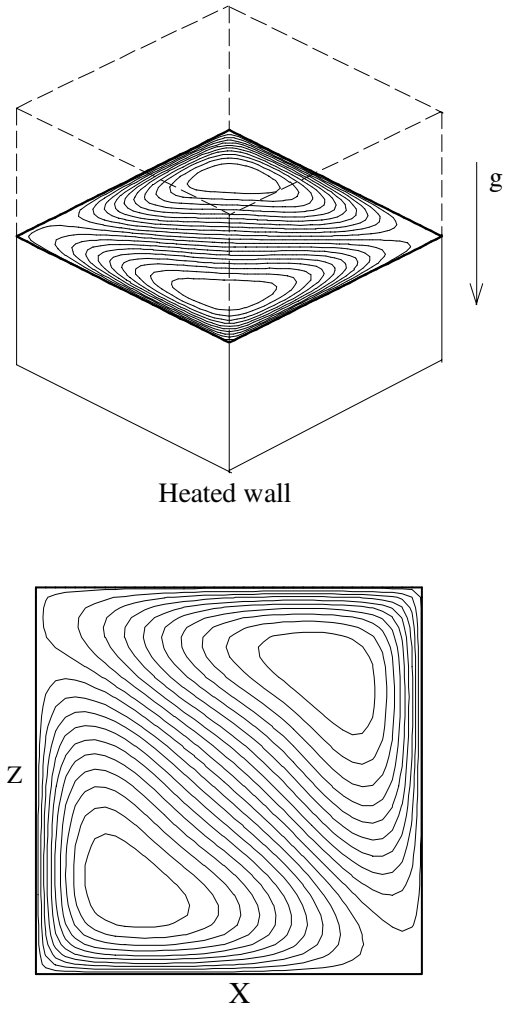

Figure 5 : Vertical velocity contours in the horizontal midplane of a cubical enclosure heated from below with adiabatic vertical walls; pattern of symmetry S_2 (Silicon, Pr=0.01, Ra=9×10^3, transitional state during the evolution that leads to S_1).

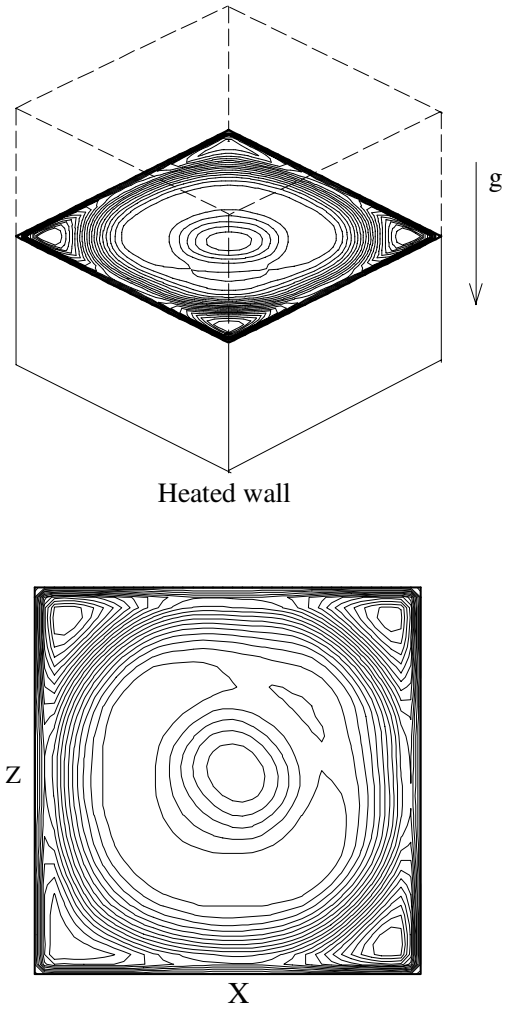

Figure 6 : Vertical velocity contours in the horizontal midplane of a cubical enclosure heated from below with adiabatic vertical walls; pattern of symmetry S_4 (Silicon, Pr=0.01, Ra=7×10^4, transitional state).

(Fig.7) consists of two asymmetric counter rotating rolls aligned along one of the $x = \pm z$ diagonals (the S_8 solution has a certain similarity to the S_2 pattern illustrated in Fig. 5).

These results are in partial agreement with the findings of Puigjaner et al. (2004); in fact, the present computations show no evidence of the other possible transitional states described by these investigators (e.g., the S_6 solution). The ranges of existence of the possible unstable regimes are also quite different. Similar discrepancies were also observed between the numerical simulations of Puigjaner et al. (2004) and available experimental results in the case of transparent organic liquids (Pallares et al., 2001 for Pr=130).

Some authors (see, e.g., the authoritative analysis of Gelfgat, 1999) tried to explain these differences in terms of some basic features of the Rayleigh-Bènard convection. It is known, in fact, that several different perturbations of the basic quiescent state can become critical at close values of the Rayleigh number; this means that in a supercritical state any of these perturbations can grow

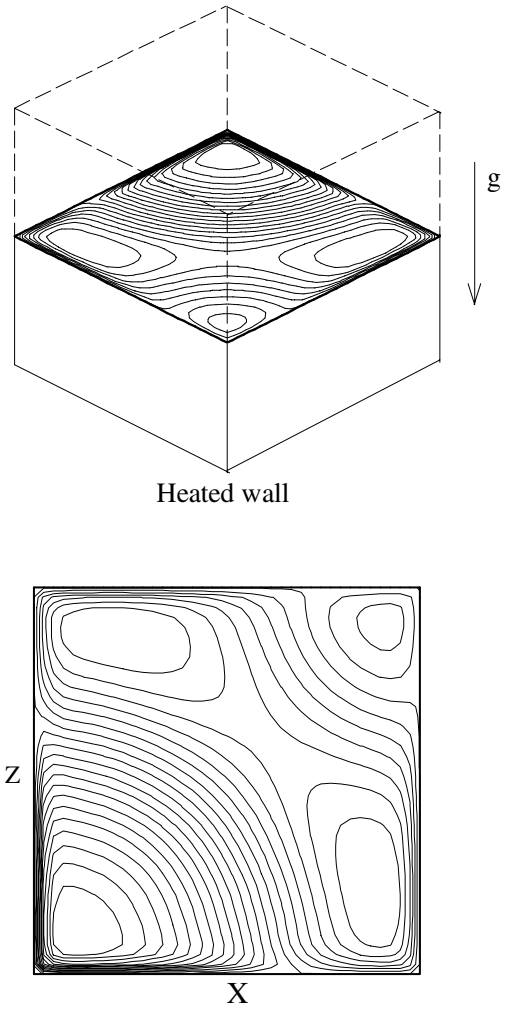

Figure 7 : Vertical velocity contours in the horizontal midplane of a cubical enclosure heated from below with adiabatic vertical walls; pattern of symmetry S_8 (Silicon, Pr=0.01, Ra=8×10^4).

and the possible states of the system will depend on the initial conditions.

The present simulations for Pr$\ll 1$ provide an additional useful point of view about these aspects.

There is indirect evidence, in fact, that another factor influencing the roll-adjustment process is the presence of thermal and/or momentum boundary layers close to the solid walls. The dynamics of these layers, in fact, completely changes according to the relative importance of transport at microscopic scale (i.e. diffusion) of momentum and energy, i.e. according to the Prandtl number.

To provide a more solid basis to these arguments it is worth spending some words about the possible existence and scaling of these zones. For instance, it is known (see e.g., Lappa, 2002) that for Pr$\leq$O(1), momentum boundary layers can develop if Gr>O(1) whose thickness scales according to $(Gr)^{-1/4}$.

Since Gr=Ra/Pr, this simple theoretical argument illustrates that the transitional dynamics of the system under investigation cannot be independent of the Prandtl number for given values of the Rayleigh number, i.e. that, even if the critical Rayleigh number for the primary bifurcation from the diffusive state is known to be not dependent on Pr, it however is not the proper parameter to put in relation possible ensuing transitional modes at different values of the Prandtl number; when convection has been initiated in the system, the dynamics of the system (i.e. its evolutionary progress) must of course depend on the presence of thermal and/or momentum boundary layers., i.e. on Pr. This argument is even more relevant when high Prandtl numbers (Pr$\gg$1) are compared to Pr=O(1) since in the first case the system is affected by the presence of thermal boundary layers whose thickness scales according to $(PrGr)^{-1/4}$whereas in the latter, the possible transitional regimes will be affected by momentum boundary layers scaling according to $(Gr)^{-1/4}$as mentioned before.

Such a theoretical argument could be used as an additional means to explain in principle the scarce reproducibility that seems to characterize this kind of experiments (e.g., the observed differences between the numerical results of Puigjaner et al. (2004) for Pr=0.710 and the experimental ones of Pallares et al. (2001) obtained for Pr=130.

3.2 Lateral heating

3.2.1 Historical background

A synthesis of available results concerning the simplified case of horizontal fluid layers of infinite extent limited from below and from above by adiabatic parallel planes, is given in the article of Hart (1983). It is shown therein that, if a velocity profile with an inflection point in the center of the layer section is assumed as representative of the basic flow in this configuration, two perturbing mechanisms (two-dimensional hydrodynamic mode with rolls perpendicular to the basic flow, three-dimensional oscillatory mode with oscillatory rolls parallel to the ba-

sic flow) are possible and that the most dangerous disturbance in the case of 0<Pr<0.033 (i.e., semiconductor melts and liquid metals) is related to the steady hydrodynamic mode. These results were refined by Kuo & Korpela (1988) who found that the first transition is to steady rolls for Pr<0.033, and to oscillatory longitudinal rolls for 0.033<Pr<0.2.

In reality, a third mechanism could be also possible if conductive thermal boundary conditions were used for the upper and lower boundaries instead of the adiabatic ones. This mode is usually referred to as the Rayleigh mode (Gershuni et al., 1992). In reality, the Rayleigh mode follows from the presence of zones of potentially unstable stratification near the upper and lower horizontal boundaries (induced by the aforementioned basic flow) that makes possible the onset of instability of the Rayleigh-Bènard type therein (steady longitudinal rolls (SLR): in practice this flow exhibits strong analogies with the convective case already discussed before in the case of uniform heating from below and for this reason it is not treated in the present section).

The hydrodynamic mode corresponds to a shear instability and is related to the formation of vortices on the frontier (i.e. close to the midsection of the layer) of the two opposing flows characterizing the basic state (i.e. close to the aforementioned inflection point); this mode is initially steady but can become time-dependent for a further increase of the temperature difference. A quite exhaustive parametric study of multiple steady states, their stability, onset of oscillatory instability, and some supercritical unsteady regimes of convective flow in two-dimensional laterally heated rectangular containers of finite extent with adiabatic upper and lower boundaries has been carried out recently by Gelfgat et al. (1999a,b) for Pr=0.015.

Many possible distinct branches of steady-state flows (pertaining to the aforementioned 2D-hydrodynamic mode) were found for this configuration. A complete study of stability of each branch was performed for the aspect ratio of the rectangular container varying continuously from 1 to 11. The results were represented as stability diagrams showing the critical parameters (critical Grashof number and the frequency at the onset of the oscillatory instability) corresponding to transitions from steady to oscillatory states, appearance of multiroll states, merging of multiple states and backwards transitions from multiroll to single-roll states.

Figs. 8 illustrate, for instance, the multiple possible steady modes of convection in a 2D laterally heated closed cavity with A= 4 for the present case of silicon melt (Pr=0.01). The single-cell structure characterized by the presence of an elongated vortex that occurs for Ra= 10^3 is taken over by a new steady state with two separate rolls when Ra is sufficiently increased (e.g., Ra=2×10^3).

Present contribution

Fig. 9a shows the three-dimensional solution corresponding to the same conditions of Fig. 8b, but with a finite width along z ($4\times1\times4$). It is evident that, unlike the multicellular flow predicted by two-dimensional studies and shown in Fig. 8b, the flow is represented by a single cell. Such a simple argument demonstrates that the presence of constraints along the third direction, like the presence of solid walls along x can play a significant role in the selection of the possible multiple states of convection with respect to the 2D case (similar conclusions were also reported by Afrid and Zebib, 1990). Furthermore, in the 3D case for Ra=2000, the flow is no longer steady and undergoes transition to an oscillatory behavior (see Figs. 9b,c); under the constraint of 2D flow (the two-roll multicellular structure in Fig. 8b), transition to time-dependence occurs for larger values of Ra (Ra=O(10^4)).

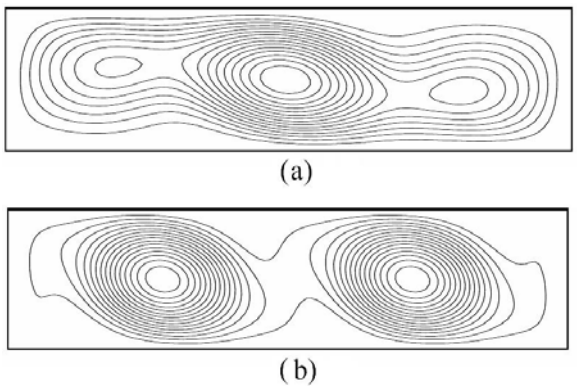

Figure 8 : Multiple steady states of two-dimensional convection in a laterally heated enclosure with A= 4 (cold and hot sides on the left and on the right of each frame, respectively, upper and lower boundaries with adiabatic conditions). Pr=0.01, silicon. Single- and two-roll steady-state flows for Ra=1×10^3(a), and Ra=2×10^3(b), respectively (Ra based on the depth of the container). For A=4, two branches of possible steady state exist.

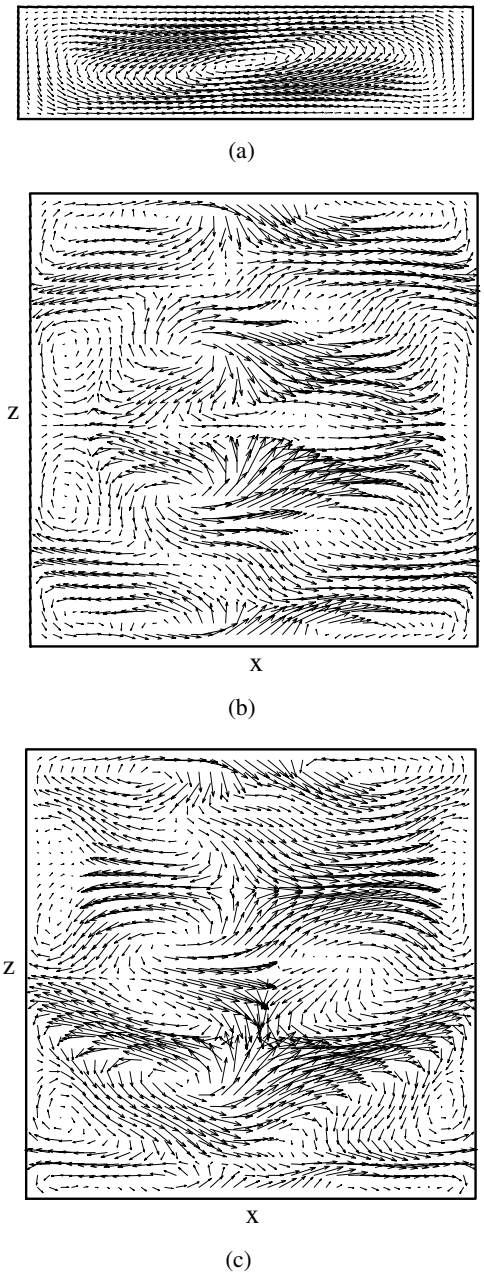

Figure 9 : Snapshots of 3D buoyancy convection in a laterally heated enclosure with $L_x = 4, L_y = 1, L_z = 4$ (Pr=0.01, silicon, Ra=2×10^3, oscillatory convection); a) xy midplane, b) and c) Projection of the velocity field in the horizontal midplane at two different times during a period of the oscillations.

In the light of these arguments, like the case of Rayleigh-Bènard convection, the presence of lateral solid constraints along the z-coordinate ($L_z/L_x \ll$O(1)) can be thought of as altering the mode selection process and the pattern symmetries.

According to the present simulations for the cubical enclosure and Pr=0.01, the three-dimensional intrinsic nature of the problem also goes beyond the effect discussed above about the deviation of the pattern-symmetry selection process in the xy plane with respect to corresponding 2D results and the threshold for the onset of time-dependence.

For this configuration, in fact, the occurrence of possible unsteady oscillations in the flow seems to be preceded by a *steady* 3D instability (Figs. 10) originated in an internal, stratified shear layer that separates from the adiabatic walls of the cavity.

Despite the immense effort provided by the scientific community over the last years (see, e.g., Roux, 1990; Kamotani and Sahraoui, 1990; Henry and Buffat, 1998, Wakitani, 2001) in the investigation of the oscillatory instabilities that can occur in these containers for Pr$\ll$1 (owing to the aforementioned theoretical kinship with the Horizontal Bridgman method) there seems to be an outstanding lack of information dealing with this primary steady bifurcation.

It is inherently three-dimensional and characterized by he presence of streamwise-oriented, counter rotating vortices.

This result seems to be in qualitative agreement with the findings of Juel et al. (2001) and Hof et al. (2004) in the case of Gallium and shallow containers. They focused on the structure of the aforementioned steady three-dimensional flow by means of experimental investigation. The three-dimensional nature of the steady flow was clearly demonstrated by quantitative experimental temperature measurements, which gave an indication of the strength of the convective flow.

According to the present simulations in the case of silicon, this three-dimensional convection is characterized by cross-flows which are an order of magnitude smaller than the main circulation, and spread from the endwall regions to the entire bulk when the Grashof number is increased beyond Gr = 5×10^3 (Fig. 10b). A couple of vortices located in the upper half of the box is also clearly visible in the yz midplane (Fig. 10c).

Within this context it is also worthwhile to stress how this instability has nothing to do with the three-dimensional flow that is usually observed in the case of experiments made with transparent (Pr$\gg$1) liquids. In such a case the

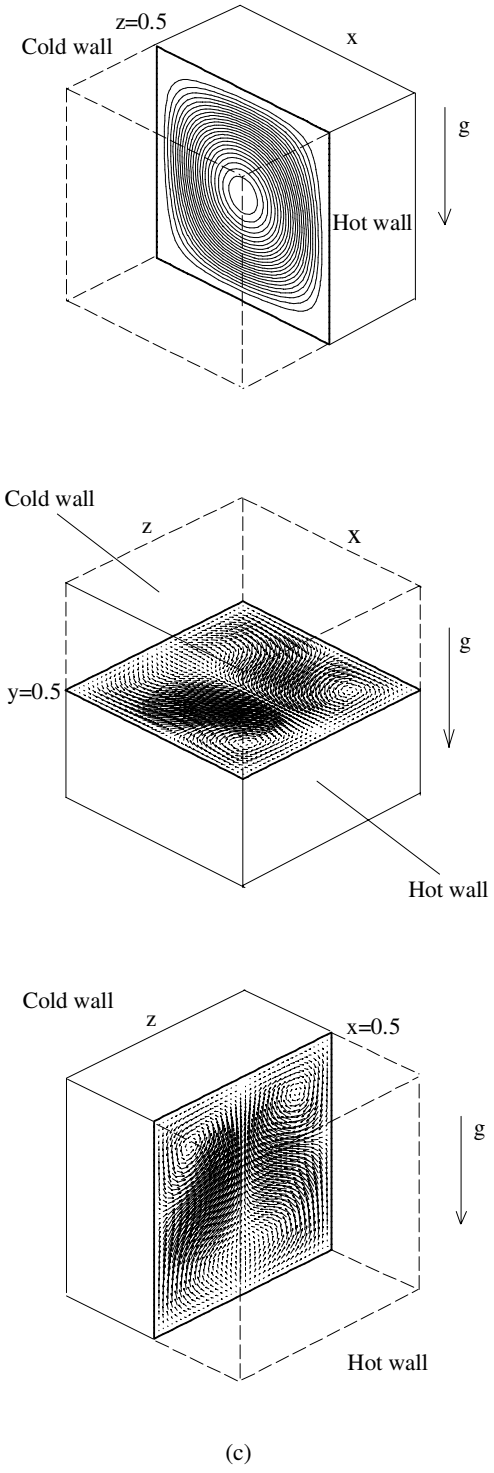

(c)

Figure 10 : Velocity field is shown in the three orthogonal coordinate planes of a cubical enclosure differentially heated from sides with adiabatic solid boundaries (Silicon, Pr=0.01, steady 3D state, Ra=10^2).

differences between the experimental flow and the idealized two-dimensional convection (see, e.g., the discussion in Hiller et al., 1989) mainly occur as a consequence of the failure to achieve strictly adiabatic condition on the insulating side walls. When idealized adiabatic boundaries are considered in the numerical simulations (see, e.g., Kowalewski, 1998) the 3D effects are somewhat limited to weak spiraling motions responsible, besides the main recirculation, for cross-flow along z (from the sidewalls towards the midplane xy).

However, for the sake of completeness it should be pointed out that steady three-dimensional flow has been also reported by means of numerical computations in the case of cubical cavities filled with air (Pr=0.710) by Fusegi et al. (1991) in a relatively wide range of the Rayleigh number and by Janssen et al. (1996). Owing to the value of the Prandtl number corresponding to air (Pr=0.710), this subject would deserve further investigation to discern the intrinsic nature of this instability for values of the Prandtl number of O(1).

3.3 Pure Marangoni flow

3.3.1 Historical background

It is well known that for small temperature differences ΔT, the flow in open cavities is steady and simply unicellular even for the case of elongated geometries. In the case of two-dimensional models, it appears as a unique large roll, whose axis is perpendicular to the temperature gradient and whose position changes according to the Prandtl number (at low Pr a recirculation roll develops near the cold wall (Fig. 11c), while at higher Pr the roll develops near the hot wall).

It is also known (Ben Hadid and Roux, 1990), that for low values of the Reynolds/Marangoni number, this fluid configuration reaches a parallel flow state in the central region (core flow) of the cavity with the exception of an upwind region (close to the hot sidewall) in which the flow is accelerated and a downwind region (close to the cold sidewall) in which the flow is decelerated (Fig. 11a). Such a parallel flow state, of course, is not present in the case of a cavities with small aspect ratio.

3.3.2 Present results

Like the case of buoyancy convection in this case the presence of sidewalls along the third direction z can lead to a variety of three-dimensional effects.

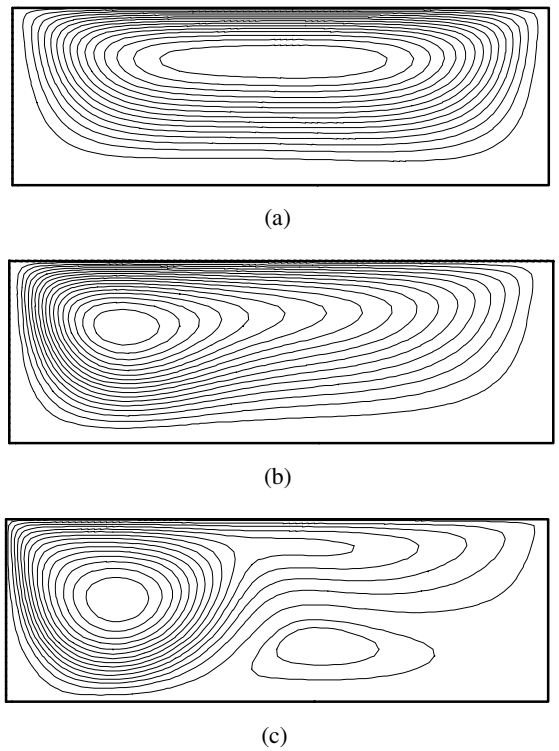

(a)

(b)

(c)

Figure 11 : Structure of pure 2D Marangoni convection for Pr=0.01 (silicon) and open cavity with aspect ratio A=3 (cold and hot sides on the left and on the right of each frame respectively, upper and lower boundaries with adiabatic conditions): (a) Ma=1, (b) Ma= 10, (c) Ma=100 (Ma based on the depth of the container).

As an example Fig. 12 provides a clear picture of the structure of the pure Marangoni flow in the three-dimensional cubical cavity (Pr=0.01 and Ma=100) already considered in the previous sections.

Vortex I represents the classical unicellular convection discussed before. Vortices (II) and (III) (see Fig. 12a) are corner vortices, that arise owing to flow separation close to solid (no-slip) boundaries (Moffatt, 1963).

Vortex (VI) and its symmetrically located counterpart are of a surface-tension-driven origin. Since the velocity component along x (i.e. u) vanishes at the solid boundaries $z = 0$ and $z = 1$, the convective transport in the x direction at the free surface is reduced there with respect to the mid-section ($z = 0.5$). This results in larger temperature values at the mid-section at fixed locations along x. Accordingly, Marangoni forces directed towards the sidewalls are induced in the z direction leading to the aforementioned well-developed secondary convective structures. The magnitude of these secondary Marangoni flows obviously tends to zero as Ma$\rightarrow$0. This is confirmed by the numerical simulations carried out for Ma=10 (not shown) where the vortices (VI) disappear.

The other secondary convective cells (IV, and V) produced by the main vortex in the vicinity of solid boundaries are Ekman structures (see Saß et al., 1995). They are somewhat similar to the secondary vortices already discussed for the case of pure buoyancy convection (Figs. 10).

At this stage it is also worthwhile to stress that the cross-flow VI, that occurs as a natural consequence of the intrinsic mechanisms of the Marangoni flow and the particular geometry considered (that leads to the onset of temperature gradients along the z direction), must not be confused with the well-known steady three-dimensional flow that can appear in liquid bridges and other models of the Floating Zone Technique under particular circumstances (Lappa, 2003, 2004b). It is known that for sufficiently small values of the Marangoni number, the convection in liquid columns of liquid metals under the effect of imposed axial temperature gradients, is laminar, steady and axisymmetrical, but when the Marangoni number exceeds certain critical values (the so-called critical Marangoni number Ma_c) depending on the Prandtl number of the liquid, on the geometry (aspect ratio), the liquid motion can undergo a transition to a steady three-dimensional (3D) complex flow pattern. In such a case the 3D flow pertains to a hydrodynamic bifurcation, and, in practice, this hydrodynamic mode corresponds to a shear instability of the shear layer below the free surface of the liquid column (see, e.g., the discussions in Lappa, 2005); hence, its nature should be regarded as similar to that of the steady bifurcation described in section 3.2 (rather than related to the 3D Marangoni flow depicted in this section).

3.4 Coupled Buoyant-Marangoni flow

The flow in the midplane $x = 0.5$ under the combined effect of buoyancy and Marangoni convection for the same cubical open cavity considered in the earlier section is illustrated in Fig. 13. Conditions at which the effects induced by both mechanisms are of comparable order of magnitude are considered (Ma=100 and Ra=1000).

According to Fig. 13, the presence of buoyancy forces dramatically increases the magnitude of the upper couple of vortices in the yz plane (previously referred to

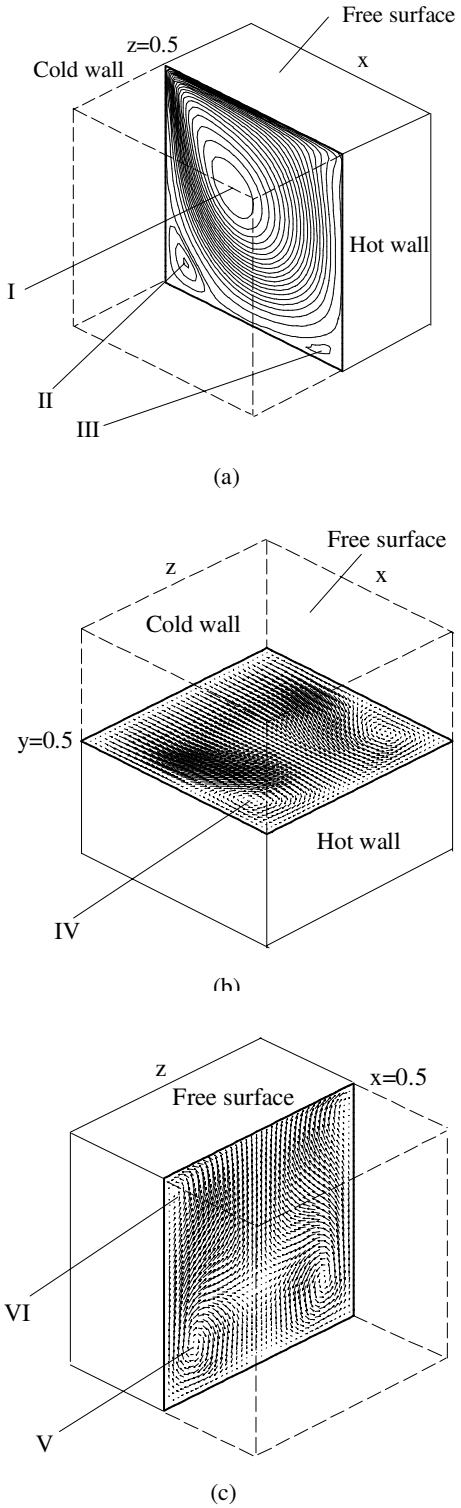

Figure 12 : Cubical cavity with free surface (Pr=0.01, Ma=100), primary and secondary vortical structures shown in the three orthogonal coordinate planes. The roman numbers are referred in the text.

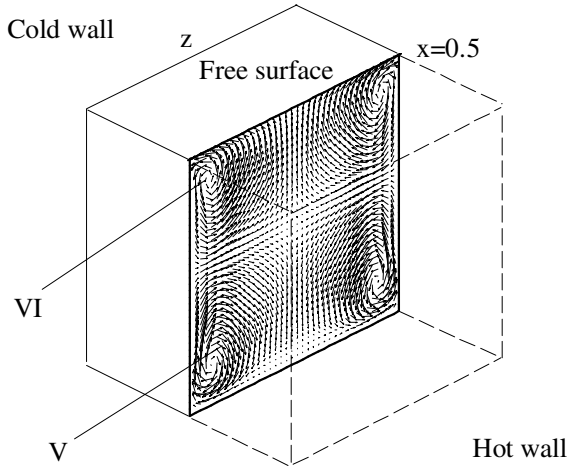

Figure 13 : Cubical cavity with free surface (Pr=0.01, Ma=100, Ra=1000), mixed buoyant-Marangoni convection in the yz midplane.

as vortices VI) leading to three-dimensional effects even more pronounced than those observed in the case of pure Marangoni convection.

Such a strengthening is, in reality, is the consequence of two separate effects:

1) The simultaneous presence of surface tension and buoyancy forces leads to a larger magnitude of the velocity on the free surface (Marangoni and buoyancy flow tend to act in the same direction along the interface); this effect, in turn, leads to an enhancement of the mechanism described in section 3.3, by which the damping effect exerted by the solid boundaries $z = 0$ and $z = 1$ on the flow can induce the onset of temperature gradients along z (that, in turn, are responsible for the presence of the vortices VI).

2) As illustrated in section 3.2, even for relatively small values of the Rayleigh number (Ra>50), the flow of buoyant origin can undergo transition to a three-dimensional pattern (shown in Figs. 10) .

These two mechanisms can support each other leading to fully-developed three-dimensional flow.

If a shallow cavity is considered (e.g., Figs. 14 deal with the case $3\times1\times3$ with Ma=100 and Ra=200) the three-dimensional cross-flow observable in the horizontal midplane is mainly due to the latter effect; for this case, in

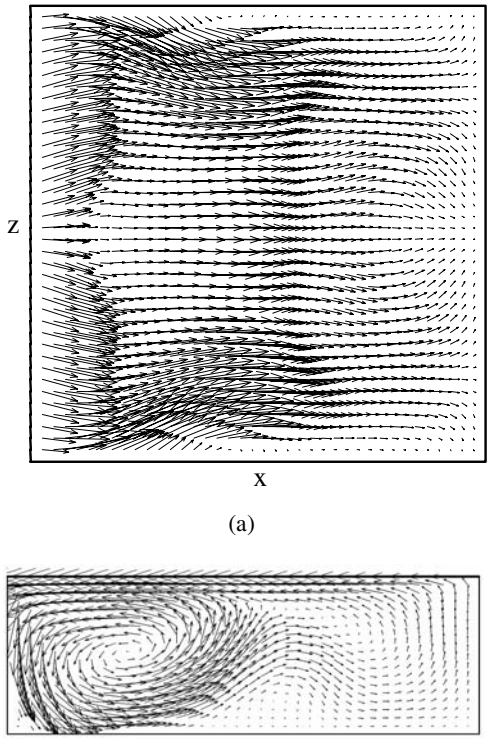

Figure 14 : mixed buoyant-Marangoni convection in the open cavity with $L_x = 3, L_y = 1, L_z = 3$ (Pr=0.01, Ma=100, Ra=200, steady state): a) Projection of the velocity field in the horizontal midplane; b) Projection of the velocity field in the *xy* midplane.

fact, the thermal mechanism discussed in section 3.3 is considerably weakened owing to the relatively large distance between the rigid walls along z (furthermore, the Ekman structures associated with the Marangoni convection do not tend to diffuse away from the lateral solid boundaries: their influence becomes very evident only when the cubical cavity or cavities with a square yz section are considered). Numerical simulations for the cavity $3\times1\times3$ in the case of pure Marangoni flow (not shown) have proven, in fact, that the structure of the convective field tends to maintain a good degree of 2D behavior even if the Marangoni number is increased to quite large values (Ma=O(10^2)).

Such a discussion also sheds some light on previous 3D results obtained by Bucchignani and Mansutti (2004) in the case of $4\times1\times1$ cavities, who attributed the onset of 3-D flow to an instability of the basic Marangoni convection. In practice, in the light of the foregoing theoretical arguments, the presence of steady three-dimensional effects in their simulation must be regarded as a non-linear effect coming from the interplay between the fundamental features of the Marangoni flow induced by the presence of side-walls along z (in particular, the surface thermal mechanism illustrated in section 3.3) and the possible (still poorly known) steady 3D buoyancy convection (described in section 3.2). In particular, as outlined before, the latter tends to be the major cause responsible for the onset of 3D flow in the case of shallow open cavities and/or pools at moderate values of the Marangoni number (e.g., the values considered in the investigation of Bucchignani and Mansutti, 2004, i.e. Ra=150 and Ma=O(100)).

For the sake of completeness, finally, it should be highlighted that steady mixed buoyant-Marangoni flows with evident 3-D features have been also found in the case of fluids with very large value of the Prandtl number (Pr$\gg$1, see, e.g., Mundrane and Zebib, 1993 and Braunsfurth and Hornsy, 1997). The underlying physics and existing theories, however, in this case, exhibit notable differences with respect to the case of Pr$\ll$1; therefore, it is necessary to open a short discussion about these aspects before going further in the description of the nature of these flows and their cause-and-effect relationships.

The oscillatory disturbances associated with the propagation of hydrothermal waves, according to the landmark analysis of Smith and Davis (1983), are known to be always the most dangerous disturbances for both cases of low and high values of the Prandtl number and "pure" Marangoni flow (i.e. microgravity conditions). For instance, by means of numerical simulations, Xu and Zebib (1998) found two-dimensional supercritical oscillatory bifurcations over a wide range of Prandtl numbers (1<Pr<13.9) and aspect ratios A; they noted that the critical threshold tends to the corresponding value predicted by Smith and Davis (1983) for the hydrothermal wave case, in the limit as $A \to \infty$. They also considered the three-dimensional case where the sidewalls located along z were found to have a damping effect on oscillations related to the propagation of the hydrothermal waves and hence increase the magnitude of the critical Ma.

However, many of the experimental results for these configurations did not provide evidence of these hydrothermal waves. In many experiments, the basic flow was observed to destabilize first against a stationary multicellular instability (transition from steady unicellular flow to

steady multicellular flow with longitudinal rolls embedded in the main flow all rotating in the same direction) before exhibiting oscillatory behaviors.

The existence of these oscillatory patterns not corresponding to the propagation of hydrothermal waves was observed by Villers and Platten (1992), De Saedeleer et al. (1996) and many others for Pr$\gg$1.

The available results in the case of transparent liquids have been summarized in the recent analysis of Burguete et al. (2001) where it is shown how depending on the height of liquid and on the extension along z, the two-dimensional basic flow destabilizes into oblique traveling waves or longitudinal stationary rolls: The first phenomenon seems to be favored for small thickness of the layer and large extension of the pool along z; vice versa the latter tends to become dominant for thick layers and small extension along z. In this case the oscillatory behavior that occurs when the thermal gradient is further increased is characterized by oscillation of the multicellular pattern.

With regard to the latter steady mode of convection, some necessary theoretical arguments (explaining its controversial existence), have been provided by the recent stability analysis of Mercier and Normand (1996). It has been clearly shown (in the case of a liquid with Pr=7) that transition between traveling waves and stationary rolls, as the most dangerous disturbances on the ground, occurs when the height of the cavity is sufficiently increased.

Within such a theoretical background, therefore, it is reasonable that the aforementioned steady 3D flow reported by Mundrane and Zebib (1993) and Braunsfurth and Hornsy (1997) for Pr$\gg$1 is somewhat an instability pertaining to the stationary rolls mode that, as explained above, tends to replace under normal gravity conditions the mechanism of propagation of hydrothermal waves predicted by Smith and Davis for pure Marangoni flows (no-g conditions). Further investigation is required along these lines.

3.5 Mixed Rayleigh-Marangoni-Bènard convection

3.5.1 Historical background

The problem concerning thin fluid layers uniformly heated from below falls into the category of phenomena known under the heading of "Marangoni-Bènard" convection. This topic is still affected by a tremendous lack of information in the case of liquid metals (with the exception of very rare efforts, see, e.g., Boeck and Thess, 1999) and is briefly treated here only for the sake of completeness since it would require much room to provide the reader with an exhaustive picture of the problem. For transparent organic liquids (e.g., silicone oils) this phenomenon, is characterized by the suggestive presence of aesthetic hexagonal cells; it is also known that at a certain distance (in terms of value of the Marangoni number) from the threshold of primary instability, square convection cells rather than the seemingly all-embracing hexagons become the persistent dominant features of this type of convection (see, e.g., Eckert et al., 1998).

3.5.2 Present results

The related mechanism in the case of pure Marangoni flow, is not treated here owing to lack of space. Rather, this section is devoted to the mixed buoyant-Marangoni problem since it, like that illustrated in section 3.4, is an even more relevant situation when this type of heated-from-below flow is encountered under normal gravity conditions.

Fig. 15 (Pr=0.01, Ra=2000, Ma=30, Bi=1) shows the Rayleigh-Marangoni-Bènard flow in the case of the $3\times1\times3$ cavity already considered in section 3.1. The cross-comparison between Figs. 3 and Figs. 15 provides additional insights into the effect that the presence of a free surface can have on the structure of the resulting buoyancy flow. According to Figs. 15a-b, in fact, the flow structure is no longer characterized by the diagonal mode of convection shown in Figs. 3; rather the hot liquid rises at the center of the cavity and the cold liquid descends along the vertical walls (toroidal structure of convection). For a further increase of the Marangoni number the flow becomes strongly time-dependent.

4 Conclusions

The different complex scenarios that arise in cubical and shallow cavities filled with silicon melt in terms of detailed structure of the convective field and possible stable and unstable regimes have been investigated within the framework of numerical solution of the non-linear balance equations through multiprocessor computations.

Significant effort has been devoted to illustrate the possible three-dimensional patterns of symmetry pertaining to various types of convective mechanisms (pure buoyancy, pure Marangoni and possible mixed states) under differ-

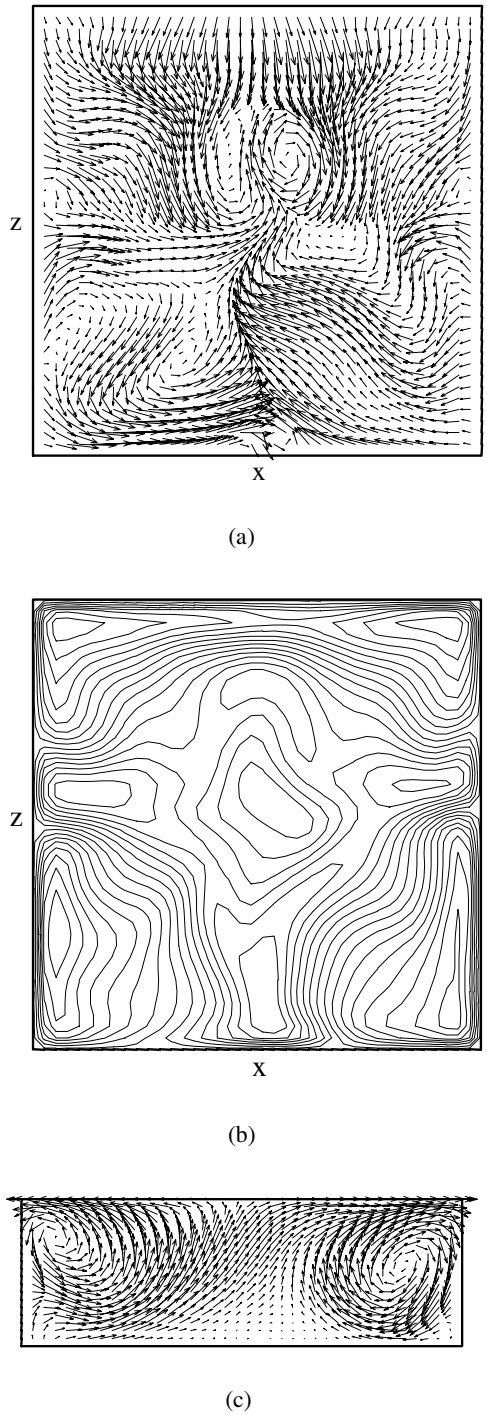

Figure 15 : Rayleigh-Marangoni-Bènard convection in an open cavity with $L_x = 3, L_y = 1, L_z = 3$ (Pr= 0.01, Ra= 2000, Ma= 30): a) Projection of the velocity field in the horizontal midplane; b) Vertical velocity contours in the horizontal midplane; c) Projection of the velocity field in the *xy* midplane.

ent heating conditions (horizontal or vertical temperature gradients) pointing out differences, analogies as well as some unexpected theoretical kinships. Critical and focused comparison with earlier two-dimensional results has been used as an additional artifice to gain additional insights into the physics of spatially limited systems. The prominent features of convective modes in these domains always tend to exhibit large sensitivity on all the possible extensions of the system if these are of a comparable measure.

Theoretical arguments supported by "ad hoc" novel and heretofore unseen numerical computations have been introduced to clarify some still unresolved discrepancies related to results provided by different investigators as well as some controversies pertaining to the driving force responsible for the observed three-dimensional flow and the physical nature of the related instability.

These studies (as well as other investigations carried out along the same lines by other researchers) are of paramount importance since they are validating new, more complex models, accelerating the current trend towards predictable and reproducible phenomena, filling gaps where existing theories are still limited to idealized systems, and finally providing an adequate scientific foundation to industrial processes which are still conducted on a largely empirical basis.

References

Afrid M. and Zebib A., (1990), Oscillatory three dimensional convection in rectangular cavities and enclosures, *Phys. Fluids*, Vol. 2, no. 9, pp. 1318-1327.

Ben Hadid H., Roux B., (1990), Thermocapillary convection in long horizontal layers of low-Prandtl number melts subject to a horizontal temperature gradient, *J. Fluid Mech.*, Vol. 221, pp. 77-103.

Boeck Th., Thess A., (1999), Bénard-Marangoni convection in low Prandtl number fluids, *J. Fluid Mech*, Vol. 399, pp 251-275.

Braunsfurth M.G. and Hornsy G. M., (1997), Combined thermocapillary-buoyancy convection in a cavity. Part II. An experimental study, *Phys. Fluids*, Vol. 9(5), pp. 1277-1286.

Bucchignani E. and Mansutti D. (2004), Rayleigh–Marangoni horizontal convection of low Prandtl number fluids, *Phys. Fluids*, Vol. 16(9), pp. 3269-3280.

Burguete J., Mukolobwiez N., Daviaud N., Garnier N., Chiffaudel A., (2001), Buoyant-thermocapillary instabilities in extended liquid layers subjected to a horizontal temperature gradient, *Phys. Fluids*, Vol. 13 (10), pp. 2773-2787.

Busse F.H., (1978), Nonlinear properties of thermal convection, *Rep. Prog. Phys.*, Vol. 41, 1929-1967.

Chandrasekhar S., (1981), Hydrodynamic and Hydromagnetic stability, Dover publications, New York.

De Saedeleer C., Garcimartin A., Chavepeyer G., Platten J.K., Lebon G. , (1996), The instability of a liquid layer heated from the side when the upper surface is open to air, *Phys. Fluids*, Vol. 8(3), pp. 670-676.

Eckert K., Bestehorn M., Thess A., (1998), Square cells in surface-tension-driven Bènard convection: experiments and theory, *J. Fluid Mech.*, Vol. 356, pp. 155-197.

Fusegi T., Hyun J.M., Kuwahara K. & Farouk B., (1991), A numerical study of three dimensional natural convection in a differentially heated cubical enclosure, *Int. J. Heat Mass Transfer*, Vol. 34(6), pp. 1543-1557.

Gelfgat A.Yu., (1999),Different Modes of Rayleigh-Benard Instability in Two- and Three-Dimensional Rectangular Enclosures, *J. Comput. Phys.*, Vol. 156, pp. 300-324.

Gelfgat A.Yu., Bar-Yoseph P.Z. and Yarin A.L., (1999a), Stability of Multiple Steady States of Convection in Laterally Heated Cavities, *J. Fluid Mech.*, Vol. 388, pp. 315-334.

Gelfgat A.Yu., Bar-Yoseph P.Z. and Yarin A.L., (1999b), Non-Symmetric Convective Flows in Laterally Heated Rectangular Cavities, *Int. J. Comput. Fluid Dynamics*, Vol. 11, pp. 261-273.

Gershuni G.Z., Laure P., Myznikov V.M., Roux B., Zhukhovitsky E.M., (1992), On the stability of plane-parallel advective flows in long horizontal layers, *Microgravity Q.*, Vol. 2, no. 3, pp. 141-151.

Hart J. E., (1983), A note on the stability of low-Prandtl-number Hadley circulations, *J. Fluid Mech.*, Vol. 132, pp. 271-281.

Henry D. and Buffat M., (1998), Two and three-dimensional numerical simulations of the transition to oscillatory convection in low-Prandtl number Fluids, *J. Fluid Mech.*, Vol. 374, pp. 145-171.

Hernández R. and Frederick R., (1994), "Spatial and thermal features of three dimensional Rayleigh–Bénard convection, *Int. J. Heat Mass Transfer*, Vol. 37, pp. 411-424.

Hiller W.J., Koch St., Kowalewski T.A., (1989), Three-dimensional structures in laminar natural convection in a cube enclosure, *Exp. Therm. and Fluid Sci.*, Vol. 2, pp. 34-44.

Hof B., Juel A., Zhao L., Henry D., Ben Hadid H., Mullin T., (2004), On the onset of oscillatory convection in molten gallium, *J. Fluid Mech*. Vol. 515, pp. 391-413.

Janssen R. J. A. and Henkens R. A. W. M., (1996), Instabilities in three-dimensional differentially heated cavities with adiabatic horizontal walls, *Phys. Fluids*, Vol. 8, no. 1, pp. 62-74.

Juel A., Mullin T., BenHadid H. and Henry D., (2001), Three-dimensional free convection in molten gallium, *J.Fluid Mech.*, Vol. 436, pp. 267-281.

Kamotani Y. and Sahraoui T., (1990), Oscillatory natural convection in rectangular enclosures filled with mercury, *J. Heat Transfer*, Vol. 112, pp. 235-255.

Kowalewski T.A., (1998), Experimental validation of numerical codes in thermally driven flows , *Adv. in Computational Heat Transfer*, pp.1-15, Begel House Inc., NY 1998.

Kuo H.P., Korpela S.A., (1988), Stability and finite amplitude natural convection in a shallow cavity with insulated top and bottom and heated from the side, *Phys. Fluids*, Vol. 31, pp. 33-42.

Lappa M., (1997), Strategies for parallelizing the three-dimensional Navier-Stokes equations on the Cray T3E, *Science and Supercomputing at CINECA*, Vol. 11, pp. 326-340.

Lappa M., (2002), Well-posed problems for the Navier-Stokes equations in the microgravity environment, *MSSU - Microgravity and Space Station Utilization*, Vol. 3, no.4, pp. 51-62.

Lappa M., (2003), Three-dimensional numerical simulation of Marangoni flow instabilities in floating zones laterally heated by an equatorial ring, *Phys. Fluids*, Vol. 15, no. 3, pp. 776-789.

Lappa M. (2004a),Fluids, Materials and Microgravity: Numerical Techniques and Insights into the Physics, *Elsevier Science* (Oxford, 2004), 538pp - ISBN 008044508X.

Lappa M., (2004b), Floating zones heated around the equatorial plane: models and simulations, *Microgravity*

Science & Technology, Vol. XV/3, pp. 36-51.

Lappa M., (2005) Thermal convection and related instabilities in models of crystal growth from the melt on earth and in microgravity: Past history and current status, *Cryst. Res. Technol*., Vol. 40, pp. 531-549.

Le Quere P., (1991), Accurate solution to the square thermally driven cavity at high Rayleigh number, *Comput*. & Fluids, Vol. 20, pp. 29–41.

Luijkx J. M., and Platten J. K., (1981), On the onset of free convection in a rectangular channel, *J. Non-Equilibrium Thermo dynam*., Vol. 6, pp. 141-149.

Mercier J. F., Normand C., (1996), Buoyant-thermocapillary instabilities of differentially heated liquid layers, *Phys. Fluids*, Vol. 8(6), pp. 1433-1445.

Moffatt H.K., (1963) Viscous and resistive eddies near a sharp corner, *J. Fluid Mech.*, Vol. 18, pp. 1-18.

Mundrane M. and A. Zebib, (1993), Two and three dimensional buoyant thermocapillary convection, *Phys. Fluids A*, Vol. 5, pp. 810-818.

Pallarès J., Arroyo M., Grau F., and Giralt F., (2001), "Experimental laminar Rayleigh–Bénard convection in a cubical cavity at moderate Rayleigh and Prandtl numbers, *Exp. Fluids*, Vol. 31, pp. 208-218.

Puigjaner D., Herrero J., Giralt F., and Simó C., (2004), Stability analysis of the flow in a cubical cavity heated from below, *Phys Fluids*, Vol.16, no. 2, pp. 3639-3655.

Roux, B., editor (1990), Numerical Simulation of oscillatory convection in low-Pr fluids, *a GAMM Workshop, Notes on numerical fluid mechanics*, vol. 27. Vieweg.

Saß V., Kuhlmann H.C. and Rath H. J., (1995), Investigation of 3D thermocapillary convection in a cubic container by a Multi-grid method, *Int. J. Heat Mass Transfer*, Vol. 39, pp. 603-613.

Smith M.K., Davis S.H. (1983), Instabilities of dynamic thermocapillary liquid layers. Part 1: convective instabilities , *J. Fluid Mech.* , Vol. 132, pp. 119-144.

Villers D., Platten J., (1992), Coupled Buoyancy and Marangoni convection in acetone: experiments and comparison with numerical simulations, *J. Fluid Mech.*, Vol. 234, pp. 487-510.

Wakitani S., (2001), Numerical study of three-dimensional oscillatory natural convection at low Prandtl number in rectangular enclosures, *J. Heat Transfer*, Vol. 123, pp. 77-83.

Xu J., Zebib A., (1998), Oscillatory two- and three-dimensional thermocapillary convection, *J. Fluid Mech.*, Vol. 364, pp. 187-209.